One-electron theory of core-level photoemission from ferromagnets

J. G. Menchero
Department of Physics, University of California at Berkeley, Berkeley, California 94720
and Materials Sciences Division, Lawrence Berkeley Laboratory, University of California, Berkeley, California 94720
(Received 18 April 1997; revised manuscript received 14 August 1997)

A one-electron theory is presented for photoemission from a p core level of a ferromagnet. The approach permits the straightforward calculation of angle- and spin-resolved photoemission spectra for an arbitrary geometry and photon polarization. The Hamiltonian employed simultaneously includes both spin-orbit and exchange interactions, and thereby accounts for mixing between the $p_{3/2}$ and $p_{1/2}$ levels. Photoelectron diffraction effects are neglected. Using this model, good agreement is obtained with experimental spin-resolved and magnetodichroic Fe $2p$ photoemission spectra.
[S0163-1829(98)09601-5]

I. INTRODUCTION

In recent years there has been great interest in utilizing core-level photoelectron spectroscopy to probe the local electronic and magnetic structure of the itinerant ferromagnets.[1–15] In the shallow $3p$ core levels, the spin-orbit and exchange interactions are approximately equal in magnitude, leading to heavy mixing between the $3p_{3/2}$ and $3p_{1/2}$ lines. This is in contrast to the deep $2p$ core levels, where the spin-orbit interaction is roughly an order of magnitude larger than the exchange interaction. As a consequence, the $2p_{3/2}$ and $2p_{1/2}$ main lines are well separated energetically, and hybridize little. These characteristics help simplify the spectroscopic interpretation, and therefore make the $2p$ core levels particularly instructive to examine.

One approach to using photoemission as a probe of magnetic systems is to directly measure the spin of the outgoing photoelectron, a method known as spin-resolved x-ray photoelectron spectroscopy (SRXPS). Due to the Pauli principle and the resulting exchange interaction, core electrons with spin parallel to the majority in the valence band will have their binding energy increased relative to electrons with spin antiparallel. This effect appears as a shift in spectral weight to higher binding energy for the majority photoelectrons. Spin-resolved studies have by now been carried out on the ferromagnetic transition metals for both the shallow core levels[1] as well as the deep core levels.[2–4] In the case of Ni, the core-level spectra exhibit prominent satellite structures with complex spin polarizations, a proper description of which requires an accurate many-body approach.[5–7] Core-level spectra of Fe and Co, on the other hand, do not exhibit such pronounced satellite structures, and one-electron theories have been used with success to describe these systems.[8–10]

An alternative to SRXPS, which does not require photoelectron spin resolution, is magnetic dichroism. The observation of magnetic dichroism in core-level photoemission was by Baumgarten *et al.*, who performed angle-resolved measurements using circularly polarized light. This technique is known as magnetic circular dichroism in the angular distribution, or MCDAD, and was used to deduce an effective exchange splitting of the Fe $2p$ main lines.[11] In MCDAD studies, two distinct methods of measurement have been employed: fixing the magnetization and reversing the photon helicity, or fixing the photon helicity and reversing the magnetization. If linear-polarized excitation is used, then dichroism can only be observed by reversal of the magnetization. This method requires angular resolution of photoelectrons, and is known as magnetic linear dichroism in the angular distributions, or MLDAD. Such dichroism was observed by Roth *et al.* in Fe $3p$ core-level photoemission.[12] It is possible to observe dichroism even with unpolarized light, an effect which can be termed MUDAD, and such studies have been carried out for several itinerant ferromagnetic systems.[13–15]

In this paper we present a one-electron theory to describe photoemission from an $l=1$ core level of a ferromagnetic system. We do not include final-state photoelectron scattering and diffraction effects, although these are by now recognized to be important when studying single-crystal samples in certain geometries.[14] In our formulation we consider an oriented atom for which the only effect of the magnetic solid is to induce an exchange splitting of the different sublevels. In addition to exchange splitting, we simultaneously include the spin-orbit interaction. Such a treatment is necessary in order to correctly describe mixing between the $p_{3/2}$ and $p_{1/2}$ levels.

Other workers have used similar approaches. For instance, Huang *et al.* also used a one-electron model which simultaneosly included both spin orbit and exchange.[10] By fitting calculated spectra to experimental observations, they were able to deduce important magnetic properties of ultrathin Fe films. In their analysis, they assumed that the radial wave functions were independent of the orbital state of the outgoing photoelectron and also that there was no interference between the $l\pm1$ channels. However, such interference is essential for the description of MLDAD phenomena.[12] Van der Laan and Cherepkov, in pioneering works, have also presented theories to describe angle-resolved core-level photoemission from ferromagnets. In van der Laan's approach,[16] the photoemission spectra are separated into two parts: one which contains the physical information, and another which depends on the geometry. Van der Laan does treat the spin-orbit and exchange interactions simultaneously, but does not, however, include spin resolution. In Cherepkov's approach,[17,18] the photoemission intensity is calculated in terms of the state multipoles and a set of parameters that describe the coupling of the various angular momenta. While Cherepkov's theory does include spin reso-

lution, it does not treat simultaneously the spin-orbit and exchange interactions, and therefore cannot account for hybridization between the $p_{3/2}$ and $p_{1/2}$ levels.

In the present paper we present a theory to describe both spin resolution *and* mixing between the levels. We also allow for a general photon incidence direction and polarization, as well as angular and spin resolution of the photoelectrons. Spin polarization resulting from cross-channel interference arises in a natural way. In the theories of van der Laan and Cherepkov, extensive use is made of angular momentum recoupling to express the photoemission intensity in terms of more fundamental quantities. Such approaches have obvious value, but lead to the introduction of many parameters which have no immediate physical interpretation. By contrast, the present approach is more straightforward and the only parameters that enter have an immediate and obvious physical meaning (e.g., photoelectron takeoff angle, photon polarization, spin-orbit and exchange energies, etc.). We believe, therefore, that the present formulation is more transparent, and will prove useful to workers in need of a direct method for calculating spin polarization and magnetic dichroism in photoemission from a p core level.

As examples, we apply our theory to Fe $2p$ SRXPS and MUDAD experimental spectra. The theory correctly reproduces the main features of the spectra, although it does not account for some details. We attribute these discrepancies to many-body effects not describable within the one-electron model considered here. In particular, we show that the experimental results suggest the existence of weak satellite structures in Fe $2p$ photoemission spectra.

II. THEORY

The electric dipole operator is defined as

$$T_\epsilon = \vec{r}\cdot\vec{\epsilon} = x\epsilon_x + y\epsilon_y + z\epsilon_z , \tag{1}$$

where $\vec{r}$ is the electron coordinate vector,

$$\vec{r} = r\hat{r} = r\left[\left(\frac{x}{r}\right)\hat{e}_x + \left(\frac{y}{r}\right)\hat{e}_y + \left(\frac{z}{r}\right)\hat{e}_z\right], \tag{2}$$

and $\vec{\epsilon}$ is the electric field polarization

$$\vec{\epsilon} = \epsilon_x\hat{e}_x + \epsilon_y\hat{e}_y + \epsilon_z\hat{e}_z . \tag{3}$$

To describe the most general photon polarization, the expansion coefficients ϵ_i must be complex. Using the usual relations for the spherical harmonics,

$$\frac{x}{r} = \sqrt{\frac{4\pi}{3}}\left(\frac{Y_1^{-1} - Y_1^1}{\sqrt{2}}\right), \quad \frac{y}{r} = i\sqrt{\frac{4\pi}{3}}\left(\frac{Y_1^1 + Y_1^{-1}}{\sqrt{2}}\right),$$

$$\frac{z}{r} = \sqrt{\frac{4\pi}{3}}Y_1^0, \tag{4}$$

we can rewrite the electron coordinate unit vector as

$$\hat{r} = \sqrt{\frac{4\pi}{3}}\left[\left(\frac{Y_1^{-1} - Y_1^1}{\sqrt{2}}\right)\hat{e}_x + i\left(\frac{Y_1^1 + Y_1^{-1}}{\sqrt{2}}\right)\hat{e}_y + Y_1^0\hat{e}_z\right] \tag{5a}$$

$$= \sqrt{\frac{4\pi}{3}}(Y_1^{-1}\hat{e}_+ - Y_1^1\hat{e}_- + Y_1^0\hat{e}_z), \tag{5b}$$

where we have introduced the circular-polarized basis vectors

$$\hat{e}_+ = \frac{\hat{e}_x + i\hat{e}_y}{\sqrt{2}}, \quad \hat{e}_- = \frac{\hat{e}_x - i\hat{e}_y}{\sqrt{2}}. \tag{6}$$

In terms of this new basis, the photon polarization vector can be rewritten

$$\vec{\epsilon} = \epsilon_+\hat{e}_+ + \epsilon_-\hat{e}_- + \epsilon_z\hat{e}_z , \tag{7}$$

where

$$\epsilon_+ = \frac{\epsilon_x - i\epsilon_y}{\sqrt{2}}, \quad \epsilon_- = \frac{\epsilon_x + i\epsilon_y}{\sqrt{2}}. \tag{8}$$

The dipole operator is then given by

$$T_\epsilon = \vec{r}\cdot\vec{\epsilon} = r\sqrt{\frac{4\pi}{3}}(-Y_1^1\epsilon_+ + Y_1^{-1}\epsilon_- + Y_1^0\epsilon_z). \tag{9}$$

This is a convenient basis for circular-polarized light propagating in the z direction, or for z-polarized light propagating along an arbitrary direction in the xy plane. However, such an expression is not immediately useful for a general polarization and geometry, as depicted schematically in Fig. 1 for an oriented atom. Here, **k** is the photoelectron wave vector, and **q** is the photon wave vector. We now proceed to generalize our development for this geometry.

The dipole operator as written in Eq. (9) is defined by six real (three complex) numbers. One of these can be related to an overall phase factor, and another can be related to a normalization condition, neither of which are important for present purposes. This leaves four remaining independent numbers to define the polarization. Due to the transverse nature of the electric field, two of these are defined by the photon propagation direction, which is given in Fig. 1 by (θ_q, ϕ_q). The other two are defined by the relative magnitude and phase difference between the two orthogonal components of the electric field. For a normalized polarization vector $\hat{\epsilon}$, this can be written in spherical coordinates in terms of two angles α and δ as

$$\hat{\epsilon} = \cos\alpha\hat{e}_\theta + \sin\alpha e^{i\delta}\hat{e}_\phi . \tag{10}$$

For Eq. (9) to be useful for a general photon polarization and propagation direction, we need to express the polarization coefficients ϵ_+, ϵ_-, and ϵ_z in terms of the four new parameters θ_q, ϕ_q, α, and δ. For a general propagation direction, the normalized dipole operator is

$$\vec{r}\cdot\hat{\epsilon} = r\sqrt{\frac{4\pi}{3}}(Y_1^{-1}\hat{e}_+ - Y_1^1\hat{e}_- + Y_1^0\hat{e}_z)(\cos\alpha\hat{e}_\theta + \sin\alpha e^{i\delta}\hat{e}_\phi), \tag{11}$$

TABLE I. Dipole operator matrix elements, $\tilde{T}_\epsilon = rY_1^1$.

$\langle\Psi_{k\uparrow}\vert$	$\langle\Psi_{k\downarrow}\vert$	$\vert j,m_j\rangle$
$-\frac{3}{2}\tilde{R}_2\sin^2\theta_k e^{2i\phi_k}$	0	$\vert\frac{3}{2},\ \frac{3}{2}\rangle$
$\sqrt{3}\tilde{R}_2\sin\theta_k\cos\theta_k e^{i\phi_k}$	$-\sqrt{\frac{3}{4}}\tilde{R}_2\sin^2\theta_k e^{2i\phi_k}$	$\vert\frac{3}{2},\ \frac{1}{2}\rangle$
$-\sqrt{\frac{1}{3}}[\tilde{R}_0+\frac{1}{2}\tilde{R}_2(3\cos^2\theta_k-1)]$	$\sqrt{3}\tilde{R}_2\sin\theta_k\cos\theta_k e^{i\phi_k}$	$\vert\frac{3}{2},\ -\frac{1}{2}\rangle$
0	$-[\tilde{R}_0+\frac{1}{2}\tilde{R}_2(3\cos^2\theta_k-1)]$	$\vert\frac{3}{2},\ -\frac{3}{2}\rangle$
$\sqrt{\frac{3}{2}}\tilde{R}_2\sin\theta_k\cos\theta_k e^{i\phi_k}$	$\sqrt{\frac{3}{2}}\tilde{R}_2\sin^2\theta_k e^{2i\phi_k}$	$\vert\frac{1}{2},\ \frac{1}{2}\rangle$
$-\sqrt{\frac{2}{3}}[\tilde{R}_0+\frac{1}{2}\tilde{R}_2(3\cos^2\theta_k-1)]$	$-\sqrt{\frac{3}{2}}\tilde{R}_2\sin\theta_k\cos\theta_k e^{i\phi_k}$	$\vert\frac{1}{2},\ -\frac{1}{2}\rangle$

where

$$\hat{e}_\theta = \cos\theta_q\cos\phi_q\hat{e}_x + \cos\theta_q\sin\phi_q\hat{e}_y - \sin\theta_q\hat{e}_z, \quad (12a)$$

$$\hat{e}_\phi = -\sin\phi_q\hat{e}_x + \cos\phi_q\hat{e}_y. \quad (12b)$$

Now using

$$(\hat{e}_\pm)^*\cdot\hat{e}_\theta = \frac{e^{\mp i\phi_q}}{\sqrt{2}}\cos\theta_q, \quad (\hat{e}_\pm)^*\cdot\hat{e}_\phi = \frac{\mp ie^{\mp i\phi_q}}{\sqrt{2}}, \quad (13)$$

we obtain the desired result:

$$\epsilon_+ = \frac{e^{-i\phi_q}}{\sqrt{2}}[\cos\alpha\cos\theta_q - i\sin\alpha e^{i\delta}], \quad (14a)$$

$$\epsilon_- = \frac{e^{i\phi_q}}{\sqrt{2}}[\cos\alpha\cos\theta_q + i\sin\alpha e^{i\delta}], \quad (14b)$$

$$\epsilon_z = -\cos\alpha\sin\theta_q. \quad (14c)$$

To illustrate the use of these relations, consider right circularly polarized (RCP) light propagating along the $+z$ direction, so that $\theta_q = 0°$. We here define RCP light to have positive helicity, which means that $\alpha = 45°$ and $\delta = 90°$, and therefore we arrive at $|\epsilon_+| = 1$. From Eq. (9), we see this corresponds to $T_\epsilon \sim Y_1^1$, i.e., the photon angular momentum is parallel to the wave vector **q**. As another example, let $\theta_q = 90°$ and $\phi_q = 0°$, so that the photon is propagating along the $+x$ direction (see Fig. 1). Suppose $\alpha = 90°$ and $\delta = 0°$, so that $\hat{\epsilon} = \hat{e}_\phi = \hat{e}_y$. Then Eq. (14) gives $\epsilon_+ = -i/\sqrt{2}$ and $\epsilon_- = i/\sqrt{2}$, so that we recover $T_\epsilon \sim i(Y_1^1 + Y_1^{-1}) \sim y$.

The α and δ defined here can also be related to the very commonly used Stokes parameters[19] by

$$s_1 = \cos 2\alpha, \quad (15a)$$

$$s_2 = \sin 2\alpha\cos\delta, \quad (15b)$$

$$s_3 = \sin 2\alpha\sin\delta, \quad (15c)$$

which gives $s_0 = \sqrt{s_1^2 + s_2^2 + s_3^2} = 1$. For a surface normal given by $\hat{n} = \hat{z}$, s_1 gives the preponderance of p-linear polarization ($\hat{\epsilon} = \hat{e}_\theta$) over s-linear polarization ($\hat{\epsilon} = \hat{e}_\phi$), with $s_1 = +1$ corresponding to p polarization and $s_1 = -1$ corresponding to s polarization. The Stokes parameter s_3 gives the preponderance of RCP over LCP light, with $s_3 = +1$ corresponding to RCP, and $s_3 = -1$ corresponding to LCP.

Let $|\Psi_{k\sigma}\rangle$ be the wave function for the outgoing photoelectron with wave vector **k** and spin σ, and let $|\Psi_{\rm core}\rangle$ be the wave function for the core electron in the initial state. The intensity is then given by

$$I_{k\sigma}^{\epsilon} = |\langle\Psi_{k\sigma}|T_\epsilon|\Psi_{\rm core}\rangle|^2\delta(E_B + E_k - \hbar\omega), \quad (16)$$

where E_B is the binding energy of the core electron, E_k is the kinetic energy of the photoelectron, and $\hbar\omega$ is the photon energy.

The final state, for emission into a general direction **k**, is given by a superposition of spherical waves[20]

$$\Psi_{k\sigma}(r,\theta,\phi) = 4\pi\sum_{lm} i^l e^{-i\delta_l}Y_{lm}^*(\theta_k,\phi_k)Y_{lm}(\theta,\phi)f_{kl}(r)\sigma, \quad (17)$$

where δ_l are the partial wave phase shifts, and $f_{kl}(r)$ are the radial wave functions at kinetic energy $E_k = \hbar^2k^2/2m$. The special case of a plane wave is recovered by setting all $\delta_l = 0$ and $f_{kl}(r) = j_l(kr)$, where $j_l(kr)$ is the spherical Bessel function of order l. In this work, we do not consider photoelectron diffraction effects in the final-state wave function, which would modify $\Psi_{k\sigma}$ further by scattering from neighboring atoms.

The initial state $\Psi_{\rm core}$ is given by

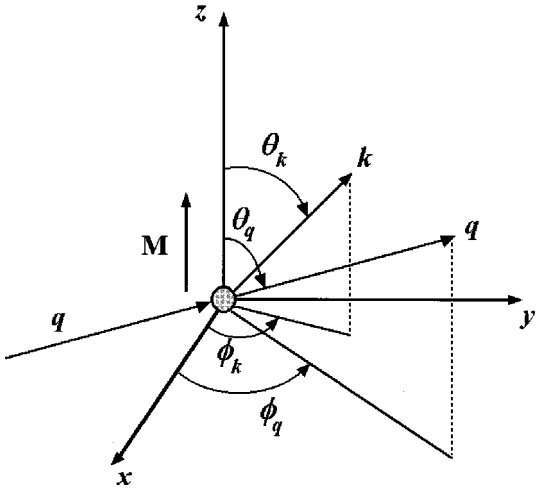

FIG. 1. General geometry. Magnetization is along the $+z$ direction. **k** and **q** are the photoelectron and photon wave vectors, respectively.

$$|\Psi_{\text{core}}\rangle = |F(r);\Phi_\sigma(\theta,\phi)\rangle, \tag{18}$$

where $F(r)$ is the radial wave function and $\Phi_\sigma(\theta,\phi)$ is the part depending on angle and spin. To determine $\Phi_\sigma(\theta,\phi)$, we follow the approach discussed by van der Laan.[16] We include the spin-orbit interaction and treat the exchange interaction by means of a spin field. The Hamiltonian is therefore given by

$$H = \lambda \vec{l}\cdot\vec{s} + \xi s_z . \tag{19}$$

As our basis states, we choose the $|j,m_j\rangle$ spin-orbit states, which can be constructed directly from the Clebsch-Gordan coefficients:

$$|3/2,\ 3/2\rangle = |Y_1^1\uparrow\rangle, \tag{20a}$$

$$|3/2,\ 1/2\rangle = \sqrt{2/3}|Y_1^0\uparrow\rangle + \sqrt{1/3}|Y_1^1\downarrow\rangle, \tag{20b}$$

$$|3/2,\ -1/2\rangle = \sqrt{1/3}|Y_1^{-1}\uparrow\rangle + \sqrt{2/3}|Y_1^0\downarrow\rangle, \tag{20c}$$

$$|3/2,\ -3/2\rangle = |Y_1^{-1}\downarrow\rangle, \tag{20d}$$

$$|1/2,\ 1/2\rangle = \sqrt{1/3}|Y_1^0\uparrow\rangle - \sqrt{2/3}|Y_1^1\downarrow\rangle, \tag{20e}$$

$$|1/2,\ -1/2\rangle = \sqrt{2/3}|Y_1^{-1}\uparrow\rangle - \sqrt{1/3}|Y_1^0\downarrow\rangle. \tag{20f}$$

The Hamiltonian in this basis then becomes

$$H = \frac{1}{6}\begin{pmatrix} 3\lambda+3\xi & 0 & 0 & 0 & 0 & 0 \\ 0 & 3\lambda+\xi & 0 & 0 & \sqrt{8}\xi & 0 \\ 0 & 0 & 3\lambda-\xi & 0 & 0 & \sqrt{8}\xi \\ 0 & 0 & 0 & 3\lambda-3\xi & 0 & 0 \\ 0 & \sqrt{8}\xi & 0 & 0 & -6\lambda-\xi & 0 \\ 0 & 0 & \sqrt{8}\xi & 0 & 0 & -6\lambda+\xi \end{pmatrix}. \tag{21}$$

The introduction of a spin field breaks the spherical symmetry, thereby mixing $j=3/2$ and $j=1/2$ levels, as evidenced by the off-diagonal terms. About the magnetization axis, however, rotational symmetry is preserved, and so m_j is still a good quantum number. In the limit $\lambda \gg \xi$ – closely realized for a $2p$ core level – the $p_{3/2}$ and $p_{1/2}$ levels are shifted energetically by $+\lambda/2$ and $-\lambda$, respectively, leading to a spin-orbit splitting of 1.5λ, and an exchange splitting of $\xi/3$ appears between adjacent m_j sublevels. The level scheme for this limit is shown in Fig. 2.

For general λ and ξ, Eq. (21) can be easily diagonalized to obtain the angular eigenstates $\Phi_\sigma(\theta,\phi)$. To calculate the matrix elements of Eq. (16) for a general initial state Ψ_{core}, it is thus sufficient to know the matrix elements for the $|j,m_j\rangle$ basis states. These have been computed for the three basic photon polarizations $\tilde{T}_\epsilon = rY_1^1$, rY_1^{-1}, and rY_1^0, and are presented in Tables I, II, and III, respectively. In these tables, θ_k and ϕ_k define the photoelectron wave vector. The $\tilde{R}_l$ are defined as $\tilde{R}_l = R_l e^{i\delta_l}$, where R_l are the radial matrix elements for the two dipole-allowed final-state channels,

$$R_l = \int_0^\infty f_{kl}(r) r^3 F(r)\, dr, \tag{22}$$

and the δ_l are the respective phase shifts. These matrix elements and phase shifts have been calculated and tabulated by Goldberg, Fadley, and Kono,[20] for several elements and energies. Note that we implicitly assumed that the radial integrals R_l are the same for both the $p_{3/2}$ and $p_{1/2}$ levels, even though the photoelectrons differ in kinetic energy and, in principle, the radial wave functions $F(r)$ may be different for the two levels. Nevertheless, such variations in R_l turn out to be quite small. For the kinetic energies of interest in XPS (above a few hundred eV), the R_l vary by only $\sim 2\%$ over an energy range corresponding to the spin-orbit splitting of a $2p$ core.[21] Furthermore, based on solutions to the Dirac equation, variations of R_l due to level-dependent radial wave functions $F(r)$ are found to be negligible.[22]

To summarize, we assume that we have an oriented atom magnetized in the z direction, as shown in Fig. 1. The photon incidence direction (θ_q,ϕ_q) and polarization (α,δ) defines the dipole operator via Eqs. (14) and (9). Dipole matrix elements between the $|j,m_j\rangle$ basis states and the outgoing photoelectron can now be determined using Tables I–III. The appropriate linear combinations of these can be formed by diagonalizing the Hamiltonian in Eq. (21), which also determines the energies of the states. Finally, Eq. (16) can be used to calculate the spin-resolved intensities of each line.

III. RESULTS AND DISCUSSION

A. Spin-resolved spectra

In Fig. 3(a) we present experimental spin-resolved spectra due to Van Campen *et al.*[2] Data were smoothed by one cycle of equal weight three-point averaging. The polycrystalline Fe sample was magnetized in-plane along what we take to be the $+z$ direction (see Fig. 1) and irradiated with a Mg Kα ($\hbar\omega = 1253.6$ eV) x-ray source. Photoelectrons were collected normal to the surface plane ($\mathbf{k} \sim \hat{e}_x$) and their spin measured along the magnetization axis. The photon $\mathbf{q}$ was defined by $\theta_q = 117°$ and $\phi_q = 142.5°$, which is a chiral geometry. To eliminate spin-orbit-induced spin polarization due to chirality, spin-resolved spectra were averaged over both magnetic orientations. In Fig. 3(a), photoelectrons with

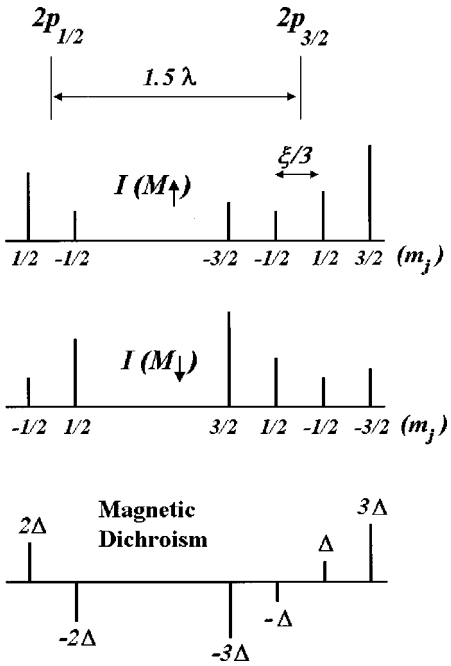

FIG. 2. Schematic diagram showing energetic positions of $|j,m_j\rangle$ core states, for both magnetic orientations, and the resulting magnetic dichroism. Such a situation is realized when the spin-orbit parameter λ is much larger than the exchange energy ξ.

spin parallel to the majority in the valence band are given by the solid line, and the corresponding minority spectrum is given by the dashed line. For both levels, an exchange splitting is clearly evident; i.e., the peak of the majority spectrum is shifted to higher binding energy. Except for the leading edge of the $2p_{3/2}$ main line, the experimental spectra show a strong majority-spin polarization throughout. Part of this is due to the spin polarization of the secondaries. To permit a more meaningful comparison with theoretical results, we subtract from the experimental results a simple linear background that eliminates the spin polarization at the leading and trailing edges. The resulting spectra are presented in Fig. 3(b). In Fig. 3(c) we present theoretical spin-resolved spectra calculated for the same experimental geometry described above, and also averaged over both magnetic orientations to eliminate spurious spin polarizations. We use a spin-orbit splitting of 13 eV ($\lambda=8.67$ eV) and a spin field of $\xi=1.20$ eV, and the resulting lines were convoluted using a Doniach-Sunjic line shape with singularity index $\alpha=0.35$ and Lorentz broadening 1.2 eV full width at half maximum (FWHM). These values were chosen to best fit the experimental line shapes and peak positions. Overall, the theoretical results are in good agreement with the background-subtracted experimental results. In Fig. 3(d), the theoretical and experimental spin polarizations are plotted. These difference spectra were normalized to the peak height of the spin-integrated intensity. The theoretical difference spectra also agree well with the main features of the experimental results, which are characterized by plus/minus features at both levels.

A more careful comparison yields the following observations.

(1) Experimentally, the main line for the majority spectrum is shifted ~ 0.5 eV to higher binding energy (relative to the minority position) for both $2p_{3/2}$ and $2p_{1/2}$. In our calculation, it is approximately 0.85 eV for $2p_{3/2}$ and 0.30 eV for $2p_{1/2}$. A more realistic treatment of the many-body interactions may account for this discrepancy. For instance, by including many-body terms in an accurate way, it was found theoretically that the energetic splittings of the $2p_{3/2}$ and $2p_{1/2}$ main lines in Ni $2p$ are approximately equal.[6]

(2) In both theory and experiment, the minority-peak intensity is enhanced at the $2p_{3/2}$ main line, and majority-peak intensity is enhanced at $2p_{1/2}$. This result is a consequence of the off-diagonal terms in Eq. (21), which lead to mixing between the $2p_{3/2}$ and $2p_{1/2}$ levels. Without such mixing, the majority- and minority-peak intensities would be equal, even though the peaks would occur at different binding energies due to exchange.

(3) Experimentally, the line shapes are spin dependent, with the line shapes for the majority photoelectrons being more asymmetrical. In other words, the majority spectrum exhibits greater strength in the high-binding-energy tail, and correspondingly less in the main line. This is especially evident for the $2p_{3/2}$ main line. Such intensity profiles are indicative of satellite structures. In Ni, such spin-dependent line shapes are also found, both experimentally[4] and theoretically,[6,7] and are a consequence of well-known satellite structures. Theoretically, the satellite is expected to have a majority-spin polarization because the mean majority satellite position is shifted to higher binding energy, and the high-binding-energy side of the satellite transfers less spectral weight to the main lines.[6,7]

B. Magnetic dichroism

In a magnetic dichroism experiment, light with a definite polarization impinges upon a magnetic sample, and the photoemission spectrum with a definite magnetization ($M\uparrow$ or $M\downarrow$) is measured as $I_{M\uparrow}$ or $I_{M\downarrow}$. In one way of measuring

TABLE II. Dipole operator matrix elements, $\tilde{T}_\epsilon = rY_1^{-1}$.

$\langle\Psi_{k\uparrow}\vert$	$\langle\Psi_{k\downarrow}\vert$	$\vert j,m_j\rangle$
$-[\tilde{R}_0+\frac{1}{2}\tilde{R}_2(3\cos^2\theta_k-1)]$	0	$\vert\frac{3}{2},\ \frac{3}{2}\rangle$
$-\sqrt{3}\tilde{R}_2\sin\theta_k\cos\theta_k e^{-i\phi_k}$	$-\sqrt{\frac{1}{3}}[\tilde{R}_0+\frac{1}{2}\tilde{R}_2(3\cos^2\theta_k-1)]$	$\vert\frac{3}{2},\ \frac{1}{2}\rangle$
$-\sqrt{\frac{3}{4}}\tilde{R}_2\sin^2\theta_k e^{-2i\phi_k}$	$-\sqrt{3}\tilde{R}_2\sin\theta_k\cos\theta_k e^{-i\phi_k}$	$\vert\frac{3}{2},\ -\frac{1}{2}\rangle$
0	$-\frac{3}{2}\tilde{R}_2\sin^2\theta_k e^{-2i\phi_k}$	$\vert\frac{3}{2},\ -\frac{3}{2}\rangle$
$-\sqrt{\frac{3}{2}}\tilde{R}_2\sin\theta_k\cos\theta_k e^{-i\phi_k}$	$\sqrt{\frac{2}{3}}[\tilde{R}_0+\frac{1}{2}\tilde{R}_2(3\cos^2\theta_k-1)]$	$\vert\frac{1}{2},\ \frac{1}{2}\rangle$
$-\sqrt{\frac{3}{2}}\tilde{R}_2\sin^2\theta_k e^{-2i\phi_k}$	$\sqrt{\frac{3}{2}}\tilde{R}_2\sin\theta_k\cos\theta_k e^{-i\phi_k}$	$\vert\frac{1}{2},\ -\frac{1}{2}\rangle$

TABLE III. Dipole operator matrix elements, $\tilde{T}_\epsilon = rY_1^0$.

$\langle\Psi_{k\uparrow}\vert$	$\langle\Psi_{k\downarrow}\vert$	$\vert j,m_j\rangle$
$\sqrt{\frac{9}{2}}\tilde{R}_2\sin\theta_k\cos\theta_k e^{i\phi_k}$	0	$\vert\frac{3}{2},\ \frac{3}{2}\rangle$
$\sqrt{\frac{2}{3}}[\tilde{R}_0-\tilde{R}_2(3\cos^2\theta_k-1)]$	$\sqrt{\frac{3}{2}}\tilde{R}_2\sin\theta_k\cos\theta_k e^{i\phi_k}$	$\vert\frac{3}{2},\ \frac{1}{2}\rangle$
$-\sqrt{\frac{3}{2}}\tilde{R}_2\sin\theta_k\cos\theta_k e^{-i\phi_k}$	$\sqrt{\frac{2}{3}}[\tilde{R}_0-\tilde{R}_2(3\cos^2\theta_k-1)]$	$\vert\frac{3}{2},\ -\frac{1}{2}\rangle$
0	$-\sqrt{\frac{9}{2}}\tilde{R}_2\sin\theta_k\cos\theta_k e^{-i\phi_k}$	$\vert\frac{3}{2},\ -\frac{3}{2}\rangle$
$\sqrt{\frac{1}{3}}[\tilde{R}_0-\tilde{R}_2(3\cos^2\theta_k-1)]$	$-\sqrt{3}\tilde{R}_2\sin\theta_k\cos\theta_k e^{i\phi_k}$	$\vert\frac{1}{2},\ \frac{1}{2}\rangle$
$-\sqrt{3}\tilde{R}_2\sin\theta_k\cos\theta_k e^{-i\phi_k}$	$-\sqrt{\frac{1}{3}}[\tilde{R}_0-\tilde{R}_2(3\cos^2\theta_k-1)]$	$\vert\frac{1}{2},\ -\frac{1}{2}\rangle$

the dichroism, the magnetization direction is simply reversed, and the difference spectrum $I_{M\uparrow}-I_{M\downarrow}$ gives the magnetic dichroism. It is instructive to consider the limit $\lambda \gg \xi$, which is approximated by a $2p$ core level in Fe. For this limit, to first order, the core eigenstates are given simply by the $\vert j,m_j\rangle$ spin-orbit eigenstates, and the energy separation between adjacent m_j sublevels is $\xi/3$. In this case, reversing the magnetization will not change the intensities of the states, but will merely interchange the energetic positions of $\vert j,m_j\rangle$ and $\vert j,-m_j\rangle$. Such a situation is shown schematically in Fig. 2. Therefore, in this limit, the magnetic dichroism for a given line is calculated simply by considering a single magnetic orientation and taking $I_{\vert j,m_j\rangle}-I_{\vert j,-m_j\rangle}$.

For RCP excitation, and the special case of photon **q** parallel to the magnetization **M**, this intensity difference is

$$2p_{3/2}: \quad I_{\vert 3/2,3/2\rangle}-I_{\vert 3/2,-3/2\rangle}=3\Delta_{\mathrm{MCDAD}}, \tag{23a}$$

$$I_{\vert 3/2,1/2\rangle}-I_{\vert 3/2,-1/2\rangle}=\Delta_{\mathrm{MCDAD}}, \tag{23b}$$

$$2p_{1/2}: \quad I_{\vert 1/2,1/2\rangle}-I_{\vert 1/2,-1/2\rangle}=2\Delta_{\mathrm{MCDAD}}, \tag{23c}$$

where Δ_{MCDAD} gives the angular distribution of the dichroism:

$$\Delta_{\mathrm{MCDAD}}=\frac{1}{3}[3R_2^2\sin^2\theta_k-R_0^2-R_2^2 - R_0R_2(3\cos^2\theta_k-1)\cos(\delta_0-\delta_2)]. \tag{24}$$

MCDAD can be qualitatively explained as a result of the spin polarization induced by circular-polarized excitation. At certain takeoff directions, there may be strong preferential emission of a given spin component—say spin up—at one of the levels. If the magnetization direction is also up, then this peak is primarily minority in character, and so is shifted to lower binding energy. When the magnetization is reversed, the spin polarization does not change (still spin up), but the peak is now majority in character and so shifts to higher binding energy, thereby leading to different spectra upon magnetic reversal.

With linear-polarized excitation, there can also be an induced spin polarization, which in turn leads to an angular-dependent magnetic linear dichroism (MLDAD). For example, let the dipole operator be given by $T_\epsilon \sim y$ (i.e., $\mathbf{q}\sim\hat{e}_x$ and $\alpha=90°$). The induced spin polarization is then

$$2p_{3/2}: \quad I_\uparrow - I_\downarrow = 2R_0R_2\sin^2\theta_k\sin 2\phi_k\sin(\delta_0-\delta_2), \tag{25}$$

$$2p_{1/2}: \quad I_\uparrow - I_\downarrow = -2R_0R_2\sin^2\theta_k\sin 2\phi_k\sin(\delta_0-\delta_2). \tag{26}$$

The magnetic dichroism is calculated in the same way as before,

$$2p_{3/2}: \quad I_{\vert 3/2,3/2\rangle}-I_{\vert 3/2,-3/2\rangle}=3\Delta_{\mathrm{MLDAD}}, \tag{27a}$$

$$I_{\vert 3/2,1/2\rangle}-I_{\vert 3/2,-1/2\rangle}=\Delta_{\mathrm{MLDAD}}, \tag{27b}$$

$$2p_{1/2}: \quad I_{\vert 1/2,1/2\rangle}-I_{\vert 1/2,-1/2\rangle}=2\Delta_{\mathrm{MLDAD}}, \tag{27c}$$

where now

$$\Delta_{\mathrm{MLDAD}}=R_0R_2\sin^2\theta_k\sin 2\phi_k\sin(\delta_0-\delta_2). \tag{28}$$

Therefore, except for an angular-dependent scaling factor, the MLDAD is equal to the MCDAD, as discussed by previous workers.[23] Although this result was derived here for a one-electron model in the limit $\lambda \gg \xi$, it holds more generally for any values of spin orbit and exchange, and is even valid for the many-body case.[23] In other words, the line shapes for both types of dichroism are identical, as shown schematically in Fig. 2.

Magnetic dichroism can also be observed with unpolarized light, which is an incoherent superposition of *s* and *p* components. Although the *s* component is nondichroic, the *p* component leads to the same dichroism as before. In Fig. 4(a) we present experimental photoemission spectra, due to Fanelsa *et al.*, for the $2p$ core of Fe (001) excited by a Mg Kα x-ray source.[14] The sample was magnetized in the surface plane, and both the photon and photoelectron wave vectors were in the plane normal to the magnetization. Photoelectron takeoff was normal to the surface and made an angle of 45° with respect to the photon incidence direction. $I_{M\uparrow}$ and $I_{M\downarrow}$ are the spin-integrated spectra for magnetization in the up and down directions, respectively. The theoretical spectra are shown in Fig. 4(b), and the difference spectra (normalized to peak intensity) are plotted in Fig. 4(c). These spectra were calculated again using $\lambda=8.67$ eV and $\xi=1.2$ eV, and the lines were convoluted with the same Doniach-Sunjic line shape as before. Overall, the theoretical results agree well with experiment, and are characterized by a plus/minus feature at $2p_{1/2}$ and a minus/plus feature at $2p_{3/2}$.

However, there are discrepancies between experiment and theory. For instance, at the $2p_{3/2}$ main line, $I_{M\uparrow}$ has a greater intensity than $I_{M\downarrow}$, whereas in the theoretical calculation they are equal. Also, the experimental dichroic signal in the interval between the main lines is much larger

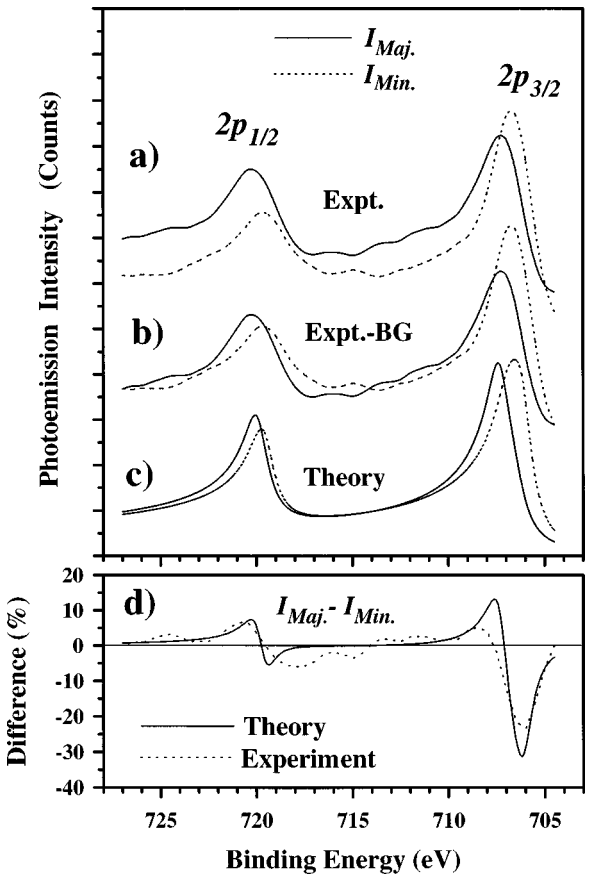

FIG. 3. Spin-resolved Fe $2p$ photoemission spectra. (a) Experimental results due to Van Campen *et al.* (Ref. 2). Data were smoothed with one cycle of the three-point averaging. (b) Background-subtracted experimental spectra. (c) Theoretical results. Lines were convoluted with a Doniach-Sunjic line shape. (d) Spin polarization, normalized to the peak intensity.

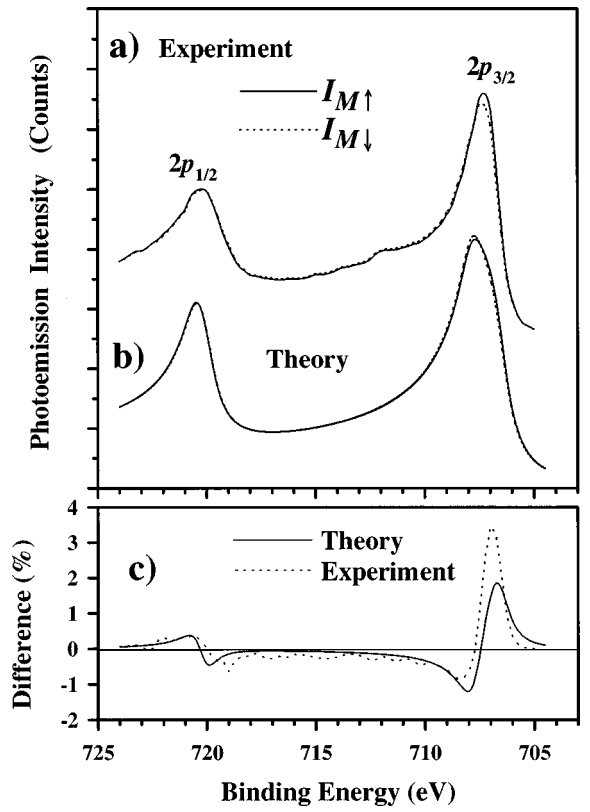

FIG. 4. Fe $2p$ magnetic unpolarized dichroism. (a) Experimental results due to Fanelsa *et al.* (Ref. 13) with spin-integrated spectra for both magnetic orientations. The small peak at 712 eV is due to satellite x rays. (b) Theoretical results. Lines were convoluted with a Doniach-Sunjic line shape with singularity index $\alpha = 0.35$ and Lorentz broadening 1.2 eV FWHM. (c) Difference spectrum for theory and experiment, normalized to the peak intensity.

than in the theoretical calculation. Both of these discrepancies may be attributed to many-body effects not accurately described within the present model. For instance, $I_{M\downarrow}$ has a majority-spin polarization at $2p_{3/2}$. The effect of satellite structures is to shift majority spectral weight to the satellite region, and away from the main line, which then acquires minority-spin polarization. This effect would explain the shape of the magnetic dichroism curve, although it cannot be modeled within the exchange-split main line approach considered here.

A direct comparison of the *magnitude* of the dichroism is not meaningful here because the experimental data were taken from a single-crystal sample. It was recently shown by Fanelsa *et al.* that photoelectron diffraction can have a strong effect on the magnitude of the dichroic asymmetry for such cases.[14]

IV. CONCLUSIONS

We have presented a one-electron theory to describe spin- and angle-resolved photoemission spectra from a p core level of a ferromagnetic system, and for a general photon polarization. We have applied the model to calculate spin-resolved Fe $2p$ spectra as well as magnetic dichroism. Agreement with experiment is generally very good. The discrepancies can be attributed to many-body effects. The spin-dependent line shapes are particularly interesting, because they are indicative of satellite structures.

ACKNOWLEDGMENTS

The author gratefully acknowledges C.S. Fadley and L.E. Klebanoff for helpful comments and stimulating discussions. Support from Lisa Borland is also greatly appreciated. This work was supported in part by the Director, Office of Energy Research, Office of Basic Energy Sciences, Materials Sciences Division of the U.S. Department of Energy under Contract No. DE-AC03-76SF00098. The author also gratefully acknowledges support during this period from the Dean's Office of U.C. Berkeley.

[1] F. U. Hillebrecht, R. Jungblut, and E. Kisker, Phys. Rev. Lett. **65**, 2450 (1990); R. Jungblut, Ch. Roth, F. U. Hillebrecht, and E. Kisker, J. Appl. Phys. **70**, 5923 (1991).
[2] D. G. Van Campen, R. J. Pouliot, and L. E. Klebanoff, Phys. Rev. B **48**, 17 533 (1993).
[3] L. E. Klebanoff, D. G. Van Campen, and R. J. Pouliot, Phys. Rev. B **49**, 2047 (1994).
[4] A. K. See and L. E. Klebanoff, Phys. Rev. B **51**, 11 002 (1995).
[5] G. van der Laan and B. T. Thole, J. Phys. Condens. Matter **4**, 4181 (1992).
[6] J. G. Menchero, Phys. Rev. Lett. **76**, 3208 (1996).
[7] J. G. Menchero, Phys. Rev. B **55**, 5505 (1997).
[8] H. Ebert, L. Baumgarten, C. M. Schneider, and J. Kirschner, Phys. Rev. B **44**, 4406 (1991).
[9] G. Rossi, F. Sirotti, N. A. Cherepkov, F. Combet Farnoux, and G. Panaccione, Solid State Commun. **90**, 557 (1994).
[10] Di-Jing Huang, D. M. Riffe, and J. L. Erskine, Phys. Rev. B **51**, 15 170 (1995).
[11] L. Baumgarten, C. M. Schneider, H. Petersen, F. Schäfers, and J. Kirschner, Phys. Rev. Lett. **65**, 492 (1990).
[12] Ch. Roth, F. U. Hillebrecht, H. B. Rose, and E. Kisker, Phys. Rev. Lett. **70**, 3479 (1993).
[13] F. U. Hillebrecht and W. D. Herberg, Z. Phys. B **93**, 299 (1994).
[14] A. Fanelsa, R. Schellenberg, F. U. Hillebrecht, E. Kisker, J. G. Menchero, A. P. Kaduwela, C. S. Fadley, and M. A. Van Hove, Phys. Rev. B **54**, 17 962 (1996).
[15] C. M. Schneider, U. Pracht, W. Kuch, A. Chasse, and J. Kirschner, Phys. Rev. B **54**, R15 618 (1996).
[16] Gerrit van der Laan, Phys. Rev. B **51**, 240 (1995).
[17] N. A. Cherepkov and V. V. Kuznetsov, J. Phys. B **22**, L405 (1989).
[18] N. A. Cherepkov, Phys. Rev. B **50**, 13 813 (1994); J. Phys. Condens. Matter **8**, 4971 (1996).
[19] J. D. Jackson, *Classical Electrodynamics* (Wiley, New York, 1975).
[20] S. M. Goldberg, C. S. Fadley, and S. Kono, J. Electron Spectrosc. Relat. Phenom. **21**, 285 (1981).
[21] A. Chasse (private communication).
[22] R. Capaz (private communication).
[23] D. Venus, Phys. Rev. B **49**, 8821 (1994); G. van der Laan and B. T. Thole, Solid State Commun. **92**, 427 (1994).